Human Molecular Genetics, 2021, Vol. 00, No. 00 1–14

https://doi.org/10.1093/hmg/ddab245
Advance Access Publication Date: 31 August 2021
General Article

GENERAL ARTICLE

Temporal dissection of Rai1 function reveals brain-derived neurotrophic factor as a potential therapeutic target for Smith–Magenis syndrome

Sehrish Javed[1,2,†], Yu-Ju Lee[1,2,†], Jin Xu[3] and Wei-Hsiang Huang[1,2,*]

[1]Department of Neurology and Neurosurgery, Centre for Research in Neuroscience, McGill University, Montréal, QC H3G 1A3, Canada, [2]Brain Repair and Integrative Neuroscience Program, The Research Institute of the McGill University Health Centre, Montréal, QC H3G 1A3, Canada and [3]State Key Laboratory of Biocontrol, School of Life Sciences, Sun Yat-Sen University, Guangzhou, China

*To whom correspondence should be addressed. Tel: 514-934-1934; Email: wei-hsiang.huang@mcgill.ca

Abstract

Haploinsufficiency of *retinoic acid-induced 1* (*RAI1*) is responsible for Smith–Magenis syndrome (SMS), a childhood neurodevelopmental disorder associated with hyperphagia, obesity and autistic features. We previously showed that constitutive inactivation of one or both copies of *Rai1* in the germline or developing brain induces SMS-like neurobehavioral deficits and obesity in mice. By contrast, the postnatal function of Rai1 is unclear. Here, we globally deleted one or both copies of *Rai1* during two postnatal developmental windows by generating an inducible *Rai1* knockout mouse model. We found that delayed *Rai1* deletion at 3 or 8 weeks of age had no effect on neurobehavioral functions but resulted in adult-onset obesity and decreased expression of brain-derived neurotrophic factor (Bdnf) in the hypothalamus. Remarkably, genetic overexpression of human Bdnf in *Rai1* heterozygous mice reversed SMS-like obesity, hyperphagia, metabolic syndrome-like features and hyposociability. Increasing Bdnf signaling in the paraventricular nucleus of the hypothalamus or the ventromedial nucleus of the hypothalamus was sufficient to mediate the anti-obesity effect. Our work identifies the function of Rai1 in different temporal windows after birth and provides *in vivo* evidence that increasing Bdnf signaling is therapeutically effective in a preclinical mouse model of SMS.

Introduction

Smith–Magenis syndrome (SMS) is caused by haploinsufficiency of *retinoic acid-induced 1* (*RAI1*) due to either point mutations in *RAI1* (1,2) or chromosomal deletions in 17p11.2 (3). SMS is characterized by hypotonia, craniofacial changes, intellectual disability, self-injurious behavior, stereotypy and autism-like features (3,4). Notably, 90% of SMS patients show hyperphagia, as well as excessive weight gain, and are above the 90th percentile in weight by early adolescence (5), a feature that persists throughout adult life. While both male and female SMS patients become obese, the latter are more likely to report overeating and appetite disorders (6). Duplication of the same 17p11.2 region is responsible for Potocki–Lupski syndrome (PTLS), a childhood neurodevelopmental disorder associated with a high incidence of autism, developmental delay and neuropsychiatric problems (7). The smallest genomic overlapping region among PTLS patients has been narrowed down to a 125 kb interval containing only *RAI1* (8). Therefore, brain development and function are sensitive to *RAI1* dosage (9).

†Equal contributions.

Received: August 2, 2020. **Revised:** August 2, 2021. **Accepted:** August 20, 2021

RAI1 is a broadly expressed transcriptional regulator (10). Human RAI1 and mouse Rai1 share highly conserved protein sequences (>80% sequence identity) (11). *Rai1*$^{+/-}$ mice are obese due to overeating and show impaired social interaction in a tube test that measures face-to-face social encounters (5,12). More than 95% of *Rai1*$^{-/-}$ mice die around embryonic day 8.5 and the few that survive develop motor dysfunction and impairment of fear learning (13). Our previous work showed that conditional removal of *Rai1* in the developing brain using a *Nestin*^{Cre} allele circumvented early embryonic lethality and recapitulated SMS-like neurobehavioral features and obesity caused by germline *Rai1* deletion (14). Transcriptomic analysis revealed that embryonic *Rai1* deletion affects the expression of hundreds of genes involved in neural circuit development and communication (5,14). Using an inducible *Rai1* reactivation allele, we further demonstrated that Rai1 reinstatement in adolescent *Rai1*$^{+/-}$ mice reverses their social dysfunction and transcriptional deficits (15). Together with the early childhood onset of SMS symptoms, this evidence suggests that Rai1 activity during early brain development is important for normal neural function. Because Rai1 is widely expressed throughout the adult brain (14), these findings also raise new questions: Is Rai1 required after neural circuits are fully developed? If so, what are the target genes downstream of Rai1 in the postnatal brain?

To determine if postnatal *Rai1* deletion recapitulates SMS-like phenotypes previously identified in mice with heterozygous and homozygous germline deletions of *Rai1* (10,12,13,15), we generated genetic mouse models in which *Rai1* was globally deleted at different postnatal stages. To our surprise, neurobehavioral functions remained intact when *Rai1* was deleted postnatally. However, delayed *Rai1* inactivation resulted in hyperphagia and obesity, which was attributed to the loss of Rai1 in neurons of the paraventricular nucleus of the hypothalamus (PVH). Rai1 maintains the expression of *Bdnf* in the postnatal hypothalamus, and overexpressing mouse *Bdnf* in neurons of the PVH or the ventromedial nucleus of the hypothalamus (VMH) was sufficient to reverse obesity in *Rai1*$^{+/-}$ mice. Remarkably, overexpressing human *Bdnf* in *Rai1*$^{+/-}$ mice reversed their body weight, overfeeding behavior, metabolic syndrome-like features and hyposociability. Collectively, the results of the present study, which dissected the function of Rai1 in a temporally and spatially specific manner, suggest that Bdnf signaling is a potential therapeutic target for SMS.

Results

Development of an adult-onset mouse model of whole-body *Rai1* deletion

To develop a postnatal onset model of Rai1 inactivation, we crossed mice carrying *Ubc*^{CreERT2}, a ubiquitously expressed, Tamoxifen (TAM)-inducible Cre allele (16), with mice carrying *Rai1*^{flox}, a *Rai1* conditional knockout allele we previously generated (14). This strategy resulted in control (*Ubc*^{CreERT2} and *Rai1*$^{flox/+}$), inducible *Rai1* heterozygous (*Ubc*^{CreERT2};*Rai1*$^{flox/+}$) and inducible *Rai1* homozygous knockout (*Ubc*^{CreERT2};*Rai1*^{CKO}) mice. To avoid the toxicity associated with repeated TAM injections (17) and to test if Rai1 expression could be effectively reduced postnatally, we performed a pilot experiment by injecting adult (8-week-old) mice with TAM (100 mg/kg) every other day for 10 days (five doses) (Fig. 1A). We performed quantitative reverse transcription polymerase chain reaction (qRT-PCR) (Fig. 1B), western blotting (Fig. 1C and D) and immunostaining (Fig. 1H) and found effective reductions in Rai1 mRNA and protein expression levels. By contrast, corn oil (vehicle) injection did not induce Rai1 loss (Fig. 1E–H).

Mice with postnatal *Rai1* deletion show normal neurobehavioral functions

Having established an effective paradigm for postnatal *Rai1* deletion, we set out to determine the importance of Rai1 at two postnatal stages: adolescence (3 weeks, when mice can survive without parental care) and adulthood (8 weeks, when mice are sexually mature) (Fig. 2A). Previous studies found that female SMS patients and *Rai1* mutant mice show more severe overfeeding and weight gain than their male counterparts (5,6,14). Therefore, we used male littermates of comparable body weight for the behavioral assays throughout our study. We injected new cohorts of control, *Ubc*^{CreERT2};*Rai1*$^{flox/+}$ and *Ubc*^{CreERT2};*Rai1*^{CKO} mice with TAM to preserve embryonic Rai1 expression and inactivate one or both copies of *Rai1* at adolescence or adulthood (Fig. 2A). We then assessed neurobehavioral function in both groups of mice 2 months after TAM injection to ensure that the phenotypes were consequent to loss of Rai1 protein. After the completion of behavioral and obesity analyses, we performed western blotting and confirmed that TAM injections reduced Rai1 protein expression in the brain (Supplementary Material, Fig. S1A and B).

To our surprise, removing Rai1 at adolescence (Fig. 2B–E) or adulthood (Fig. 2F–I) did not induce SMS-like neurobehavioral phenotypes. We and others have previously reported that mice with germline *Rai1* heterozygous deletion show a significant decrease of social interaction in the tube test (12,15). However, heterozygous deletion of *Rai1* in adolescence or adulthood did not interfere with social interaction (Fig. 2B and F). Germline *Rai1* homozygous deletion also results in more than 95% of the mice dying during gastrulation and organogenesis (10). The few surviving *Rai1*$^{-/-}$ mice exhibit decreased motor function in the pole test and learning impairment in a Pavlovian fear-conditioning task (13). By contrast, *Ubc*^{CreERT2};*Rai1*^{CKO} mice with TAM injected at 3 or 8 weeks of age acquired proper motor function (Fig. 2C and G), normal acquisition of conditioned fear (Fig. 2D and H), and intact cued and contextual recall (Fig. 2E and I). These results suggest that postnatal Rai1 activity is dispensable for neurobehavioral functions.

To ensure that our experimental paradigm was sensitive enough to detect behavioral changes associated with decreased *Rai1* expression, we deleted *Rai1* from the embryonic brain by crossing *Nestin*^{Cre} mice (18) with *Rai1*^{flox} mice and generated control (*Nestin*^{Cre} and *Rai1*$^{flox/+}$), *Rai1* heterozygous knockout (*Nestin*^{Cre};*Rai1*$^{flox/+}$) and *Rai1* homozygous knockout (*Nestin*^{Cre};*Rai1*^{CKO}) mice (Supplementary Material, Fig. S2A). Western blotting confirmed reduced Rai1 expression in the brain (Supplementary Material, Fig. S2B). We found that 8-week-old *Nestin*^{Cre};*Rai1*$^{flox/+}$ mice showed impaired social interaction in the tube test (Supplementary Material, Fig. S2C). Furthermore, *Nestin*^{Cre}; *Rai1*^{CKO} mice showed motor dysfunction in the pole test (Supplementary Material, Fig. S2D), impaired acquisition of conditioned fear (Supplementary Material, Fig. S2E) and reduced cued and contextual recall of conditioned fear (Supplementary Material, Fig. S2F). These SMS-like behavioral deficits are consistent with previous findings in *Rai1* germline and pan-neural *Rai1* heterozygous and homozygous knockout mice (12,13,15) and indicate that the lack of behavioral deficits in postnatal *Rai1* knockout mice (Fig. 2) was not due to insufficient sensitivity in our behavioral tests. It should be noted that the results obtained from the global (*Ubc*^{CreERT2}) and brain-specific

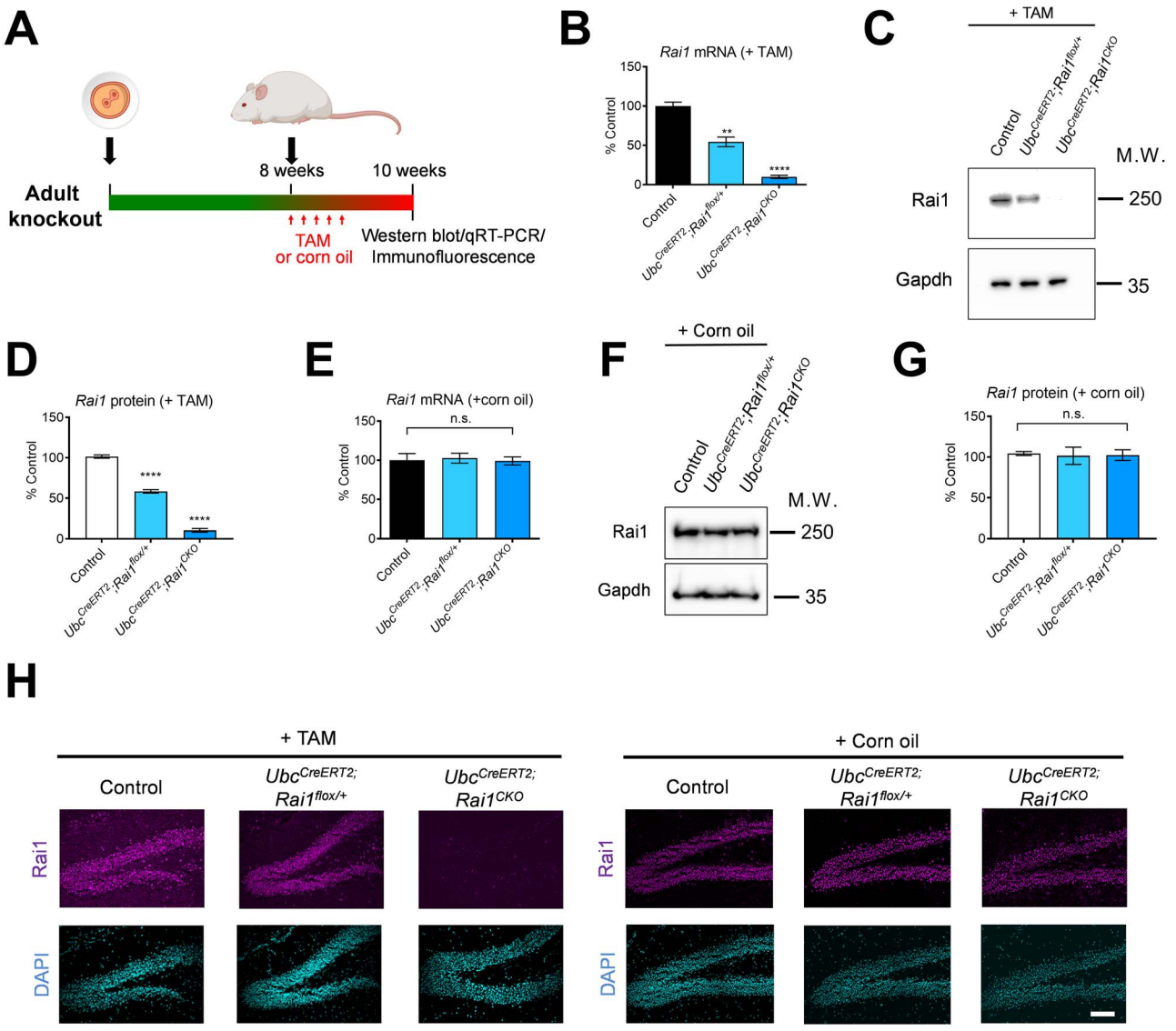

Figure 1. TAM-induced *Rai1* deletion in adult mice. (**A**) Schematic depicting *Rai1* deletion in adulthood by five doses of TAM injections starting at 8 weeks of age over 10 days. Hypothalamic tissues were harvested at 10 weeks of age to detect Rai1 mRNA and protein expression. (**B**) qRT-PCR showing that TAM injections reduced *Rai1* mRNA expression ($n = 3$ per genotype). (**C**) Western blot data indicating that TAM injections reduced Rai1 protein expression. Gapdh was used as a loading control. M.W., molecular weight. (**D**) Western blot quantification of Rai1 protein levels relative to control mice after TAM injections ($n = 3$ per genotype). (**E**) qRT-PCR showing that corn oil (vehicle) injections did not significantly alter *Rai1* mRNA expression ($n = 3$ per genotype). (**F**) Western blot data showing that corn oil (vehicle) injections did not alter Rai1 protein expression. (**G**) Western blot quantification of Rai1 protein levels relative to control mice after corn oil injections ($n = 3$ per genotype). The data in B, D, E and G are shown as means (±SEM). n.s. indicates not significantly different. $^{****}P < 0.0001$. (**H**) TAM but not corn oil injections noticeably reduced Rai1 protein expression in the dentate gyrus of $Ubc^{CreERT2}$;$Rai1^{CKO}$ mice. Scale bars: 100 µm.

($Nestin^{Cre}$) Cre lines should be interpreted with caution due to their differences in inducing both the temporal and spatial patterns of *Rai1* deletion.

To further determine if postnatal *Rai1* deletion induced a late-onset behavioral phenotype, mice with *Rai1* deleted at adolescence were retested for social interaction and motor function at 7–8 months of age (Supplementary Material, Fig. S3A). At this age, $Ubc^{CreERT2}$;$Rai1^{flox/+}$ and $Ubc^{CreERT2}$;$Rai1^{CKO}$ mice weighed significantly more than their age-matched control littermates but showed normal neurobehavioral functions (Supplementary Material, Fig. S3B–D). Together with previous findings, these results suggest that neural circuits important for motor function, social behavior and learning were not affected by global deletion of *Rai1* beyond weaning age.

Postnatal *Rai1* deletion results in abnormal gene expression and recapitulates SMS-like hyperphagia and obesity

Obesity associated with hyperphagia is a major disabling feature of SMS, especially for female patients (5,6). This led us to closely examine the body weight of mice to determine if Rai1 activity at different postnatal windows is required to maintain energy homeostasis. In contrast to the finding that postnatal Rai1 expression is dispensable for neurobehavioral functions, we found that both heterozygous and homozygous *Rai1* deletion at 3 weeks of age induced dose-dependent obesity in female mice (Fig. 3A). Furthermore, deleting two copies (but not one copy) of *Rai1* at 8 weeks of age also induced a significant

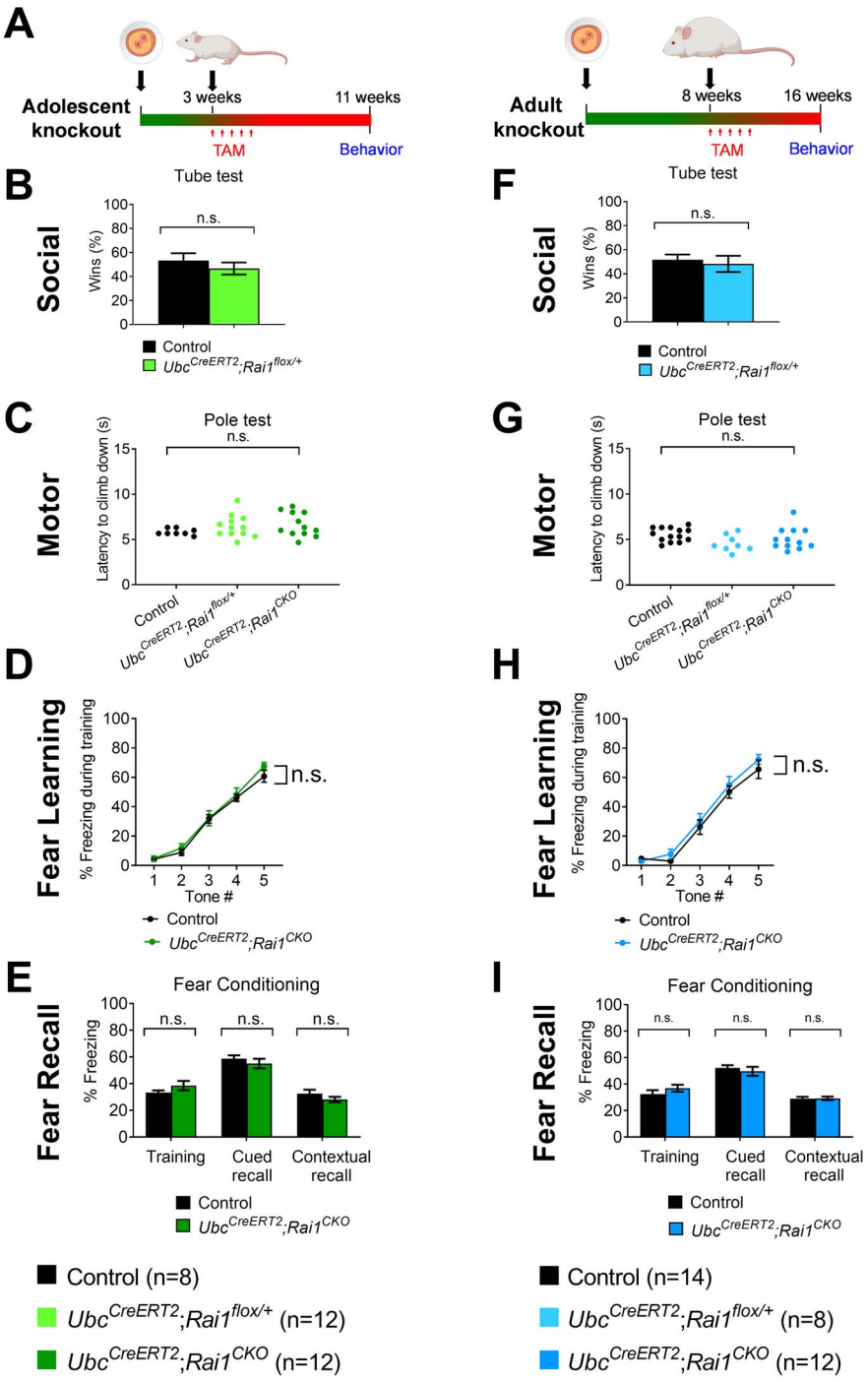

Figure 2. Mice with *Rai1* deleted at adolescent or adult stages show normal neurobehavioral function. (**A**) Schematic depicting *Rai1* deletion during adolescence (3 weeks) or adulthood (8 weeks). The fertilized egg indicates conception. (**B**) $Ubc^{CreERT2}$;$Rai1^{flox/+}$ mice showed normal social interaction upon TAM injections in adolescence. (**C**) In the pole test, $Ubc^{CreERT2}$;$Rai1^{flox/+}$ and $Ubc^{CreERT2}$;$Rai1^{CKO}$ mice showed normal motor function when *Rai1* was deleted in adolescence. (**D**) $Ubc^{CreERT2}$;$Rai1^{CKO}$ mice showed normal acquisition of fear conditioning when *Rai1* was deleted in adolescence. (**E**) $Ubc^{CreERT2}$;$Rai1^{CKO}$ mice also showed normal cued and contextual recall in a fear conditioning task when *Rai1* was deleted in adolescence. (**F**) $Ubc^{CreERT2}$;$Rai1^{flox/+}$ mice showed normal social interaction upon TAM injections in adulthood. (**G**) $Ubc^{CreERT2}$;$Rai1^{flox/+}$ and $Ubc^{CreERT2}$;$Rai1^{CKO}$ mice showed normal motor function upon TAM injections in adulthood. (**H** and **I**) $Ubc^{CreERT2}$;$Rai1^{CKO}$ mice showed normal acquisition of conditioned fear, as well as cued and contextual recall of learned fear, when *Rai1* was deleted in adulthood. n.s. indicates not significantly different. Error bars indicate SEM. Asterisks indicate the effect of genotype.

weight gain (Fig. 3B). Fifteen weeks after the last dose of TAM, $Ubc^{CreERT2}$;$Rai1^{CKO}$ mice injected with TAM at adolescence or adulthood weighed 34 or 22% more than their respective control littermates (Supplementary Material, Fig. S4A and B). In male mice, we also found that heterozygous and homozygous *Rai1* loss in adolescence as well as homozygous (but not heterozygous) *Rai1* loss in adulthood induced late-onset obesity (Fig. 3C–D). This suggests that postnatal Rai1 activity regulates

energy balance in both sexes. Increased body weight could be caused by many factors, including food intake and energy expenditure (EE). We and others have shown that embryonic deletion of *Rai1* increases food intake but does not affect EE (5,14). Similarly, $Ubc^{CreERT2}$;$Rai1^{CKO}$ mice showed increased food intake 15 weeks after the last dose of TAM (Fig. 3E). As expected, the body weight of corn oil-treated $Ubc^{CreERT2}$;$Rai1^{CKO}$ mice remained similar to that of control littermates (Supplementary Material, Fig. S4C), consistent with the lack of non-specific *Rai1* deletion.

The continuous requirement of Rai1 in maintaining body weight homeostasis throughout life led us to hypothesize that Rai1 regulates a similar set of genes that control food intake in the developing and adult hypothalamus (19). Therefore, we harvested hypothalamic tissues from $Ubc^{CreERT2}$;$Rai1^{CKO}$ mice and their control ($Ubc^{CreERT2}$) littermates injected with TAM at adolescence and performed RNA sequencing (Supplementary Material, Fig. S5A). We found that among 73 differentially expressed genes, 47 were downregulated and 26 were upregulated upon postnatal deletion of *Rai1* (Supplementary Material, Fig. S5B and Supplementary Material, Table S1). Gene ontology analysis showed that downregulated genes were involved in cellular responses to signaling and transcription (Fig. 3F–G). To identify misregulated genes shared between early and postnatal *Rai1* deletion, the hypothalamic transcriptome of postnatal *Rai1* knockout mice was compared to our published hypothalamic transcriptome of $Vglut2^{Cre}$;$Rai1^{CKO}$ mice, which become obese due to embryonic loss of Rai1 in subcortical excitatory neurons (14). While the majority of differentially expressed genes were distinct when *Rai1* was deleted at different time points, we identified three commonly downregulated genes (FDR < 0.1): *Bdnf*, *calbindin-1* (*Calb1*) and *netrin G1* (*Ntng1*) (Fig. 3H). Decreased *Bdnf* expression was validated using qRT-PCR (Supplementary Material, Fig. S5C). Because decreased *Bdnf* expression increases food intake and results in obesity in humans and mice (20–23), our findings suggest that Rai1 is potentially required for central control of energy balance through the maintenance of postnatal *Bdnf* expression.

Ectopic *Bdnf* expression in selective hypothalamic nuclei reverses SMS-like obesity phenotype

Our transcriptomic analysis suggests that postnatal loss of Rai1 causes aberrant transcriptional changes in the hypothalamus. Multiple hypothalamic nuclei including the PVH neurons express *Bdnf* (24). Interestingly, we previously found that $Sim1^{Cre}$-mediated *Rai1* deletion induces obesity in mice (14). Because $Sim1^{Cre}$ is expressed in multiple brain regions, including the medial amygdala, nucleus of the lateral olfactory tract, supraoptic and posterior hypothalamic nuclei, and PVH (25), the identity of the neurons mediating obesity in *Rai1* mutant mice remains unclear. Therefore, we set out to evaluate the contribution of the PVH to the obesity phenotype caused by postnatal Rai1 loss using adeno-associated virus (AAV). To test if AAV-mediated Cre expression could effectively delete *Rai1* in the hypothalamus, we unilaterally injected AAV into the PVH to express Cre-GFP in 3-week-old $Rai1^{flox/flox}$ mice. Immunostaining showed that in the injected side of the PVH, GFP^+ cells did not express Rai1, whereas in the control side, GFP-negative PVH neurons expressed Rai1 (Fig. 4A). Having validated that AAV-Cre-GFP could efficiently delete *Rai1* in the PVH, we bilaterally injected AAVs expressing GFP only (control) or Cre-GFP into 3-week-old female $Rai1^{flox/flox}$ mice (Fig. 4B). We observed a significant gain in body weight for $Rai1^{flox/flox}$ mice injected with AAV-Cre-GFP but not for those injected with AAV-GFP (Fig. 4C). This observation is consistent with the view that Rai1 has an ongoing role in PVH neurons to mediate body weight homeostasis and independently confirmed our findings that postnatal Rai1 activity is necessary to prevent obesity.

Postnatal deletion of *Bdnf* from PVH neurons drives obesity in mice (24). To determine if enhancing *Bdnf* signaling could reverse the obesity caused by *Rai1* haploinsufficiency, AAVs expressing GFP alone or both GFP and mouse Bdnf (AAV9-CMV-GFP-2A-mBdnf) were stereotaxically injected into the PVH of 4-week-old $Rai1^{+/-}$ mice (hereafter, SMS mice) generated by crossing germline Cre ($ActB^{Cre}$) mice with $Rai1^{flox/flox}$ mice (Fig. 4D). AAV-GFP and AAV-GFP-mBdnf were also injected into the PVH of control mice ($ActB^{Cre}$). Immunostaining using anti-Bdnf and anti-GFP antibodies confirmed the ectopic expression of mBdnf in PVH neurons (Fig. 4E). While SMS mice injected with AAV-GFP were obese compared to control mice injected with AAV-GFP, intriguingly, the body weight of SMS mice injected with AAV-GFP-2A-mBdnf was significantly lower than that of SMS mice injected with AAV-GFP and was indistinguishable from that of control mice injected with AAV-GFP or AAV-GFP-2A-mBdnf (Fig. 4F). These results suggest that AAV-mediated mBdnf overexpression in the PVH reversed the body weight phenotype caused by germline *Rai1* heterozygous deletion. To test if overexpressing mBdnf in other hypothalamic neurons could reverse the obesity in SMS mice, AAVs encoding GFP or GFP-mBdnf were stereotaxically injected into the VMH (Supplementary Material, Fig. S5D), which is enriched with neurons that produce Bdnf to suppress appetite (26,27). We previously reported that deleting *Rai1* from $SF1^{Cre}$-lineage neurons (including VMH neurons) causes obesity (14,28). Interestingly, SMS mice expressing AAV-GFP-2A-mBdnf (but not SMS mice expressing AAV-GFP) were similar in body weight to control mice expressing AAV-GFP (Supplementary Material, Fig. S5E), suggesting that overexpressing mBdnf in VMH neurons also corrects SMS-like obesity in mice. Control mice overexpressing AAV-GFP-2A-mBdnf in the VMH also showed decreased body weight, suggesting that PVH and VMH neurons may respond differently to mBdnf overexpression. Altogether, these experiments suggest that an exogenous supply of mBdnf reversed obesity in 4-week-old SMS mice through PVH and VMH neurons: the two major groups of neurons responsible for the effect of Bdnf on energy homeostasis (29).

Ectopic expression of human *Bdnf* reverses SMS-like obesity and metabolic features in SMS mice

Bdnf has emerged as a promising molecular target to treat neurological, psychiatric and obesity disorders (30). To explore the therapeutic potential of Bdnf in SMS, we tested if genetically overexpressing human Bdnf (hBdnf) could reverse obesity and metabolic phenotypes caused by *Rai1* haploinsufficiency (5,12,15). To simultaneously delete one copy of *Rai1* in the germline (i.e. to mimic SMS pathogenesis) and ectopically express hBdnf, we crossed $ActB^{Cre}$ mice with germline Cre activity (31), *Rai1-flox* mice and *Bdnf-STOP* mice that express *hBdnf* in a Cre-dependent manner (32). This crossing scheme resulted in control mice ($ActB^{Cre}$), SMS mice ($ActB^{Cre}$;$Rai1^{flox/+}$), *Bdnf*-overexpressing mice ($ActB^{Cre}$;$Bdnf^{STOP/+}$; hereafter $hBdnf^{Tg}$) and SMS mice with *hBdnf* overexpressed ($ActB^{Cre}$;$Rai1^{flox/+}$;$Bdnf^{STOP/+}$; hereafter SMS + $hBdnf^{Tg}$) (Fig. 5A). We performed qRT-PCR and confirmed that compared to control mice, *Rai1* mRNA levels in SMS mice with or without hBdnf treatment decreased by 50% (Fig. 5B, left panel). Using a primer set that recognizes both human and mouse *Bdnf*, we confirmed Cre-dependent overexpression of *Bdnf* (a 2.7-fold increase compared to control),

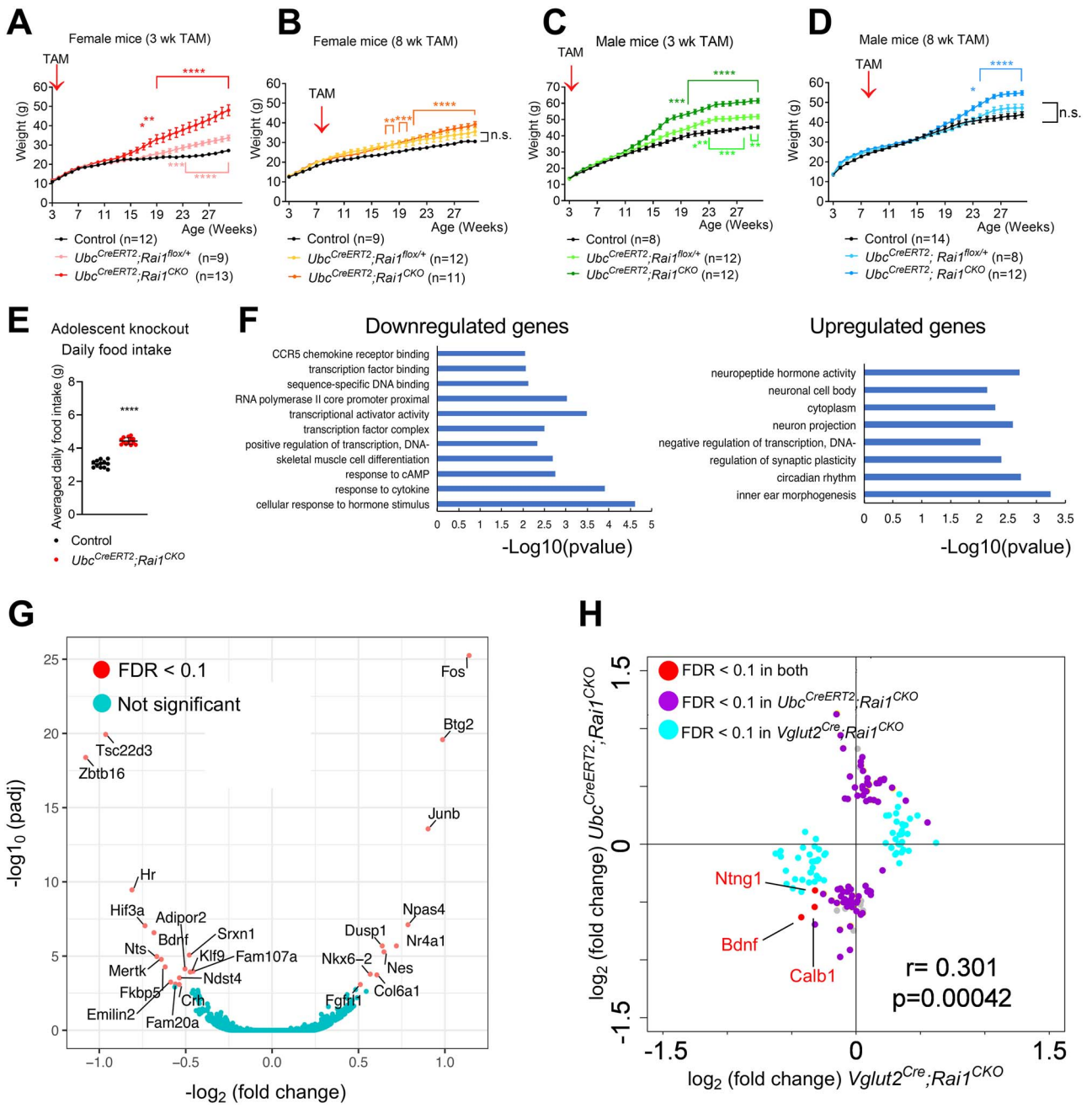

Figure 3. *Rai1* deletion in adolescent and adult mice induces obesity. (**A**) TAM injections at 3 weeks of age induced obesity in female $Ubc^{CreERT2}$;$Rai1^{flox/+}$ and $Ubc^{CreERT2}$;$Rai1^{CKO}$ mice when compared to control ($Ubc^{CreERT2}$ and $Rai1^{flox/+}$) mice. (**B**) TAM injections at 8 weeks of age induced obesity in female $Ubc^{CreERT2}$;$Rai1^{CKO}$ but not $Ubc^{CreERT2}$;$Rai1^{flox/+}$ mice. (**C**) TAM injections at 3 weeks of age induced obesity in male $Ubc^{CreERT2}$;$Rai1^{flox/+}$ and $Ubc^{CreERT2}$;$Rai1^{CKO}$ mice. (**D**) TAM injections at 8 weeks of age induced obesity in male $Ubc^{CreERT2}$;$Rai1^{CKO}$ but not $Ubc^{CreERT2}$;$Rai1^{flox/+}$ mice. The data in A, B, C and D show the mean body weight, where error bars indicate the SEM. n.s. indicates not significantly different. $^{*}P < 0.05$, $^{**}P < 0.01$, $^{***}P < 0.001$, $^{****}P < 0.0001$. (**E**) Averaged daily food intake of female $Ubc^{CreERT2}$;$Rai1^{CKO}$ mice (adolescent knockout) and their control littermates. Food intake was monitored over 7 days and averaged to obtain daily intake. Each dot indicates one mouse. (**F**) Gene ontology analysis indicating that differentially expressed genes induced by postnatal *Rai1* deletion were involved in cellular responses and transcription. In contrast, our previous findings when *Rai1* was deleted in the embryonic stage showed the involvement of neurodevelopmental genes (14). (**G**) Volcano plot of RNA-sequencing results of 30-week-old control ($Ubc^{CreERT2}$) and $Ubc^{CreERT2}$;$Rai1^{CKO}$ hypothalamic tissues with TAM injected at adolescence. Genes marked in red (FDR < 0.1) were significantly misregulated in $Ubc^{CreERT2}$;$Rai1^{CKO}$ mice. (**H**) Misregulated genes in the $Ubc^{CreERT2}$;$Rai1^{CKO}$ mice with TAM injected in the adolescent stage (purple dots) and female $Vglut2^{Cre}$;$Rai1^{CKO}$ hypothalamus [blue dots, from Huang *et al.* (14)]. Red dots indicate commonly downregulated genes (FDR < 0.1).

consistent with previous findings (32). SMS mice without hBdnf treatment showed a 40% decrease in *Bdnf* expression compared to control mice (Fig. 5B, right panel, red versus black bars), which was reversed after hBdnf treatment and showed a 97% increase compared to control mice (Fig. 5B, blue versus black bars). Together, these findings confirmed that ectopic hBdnf expression did not affect the Rai1 levels but increased Bdnf expression in SMS mice.

Next, we monitored the body weight of these mice weekly. Instead of becoming obese, the body weight of SMS mice treated

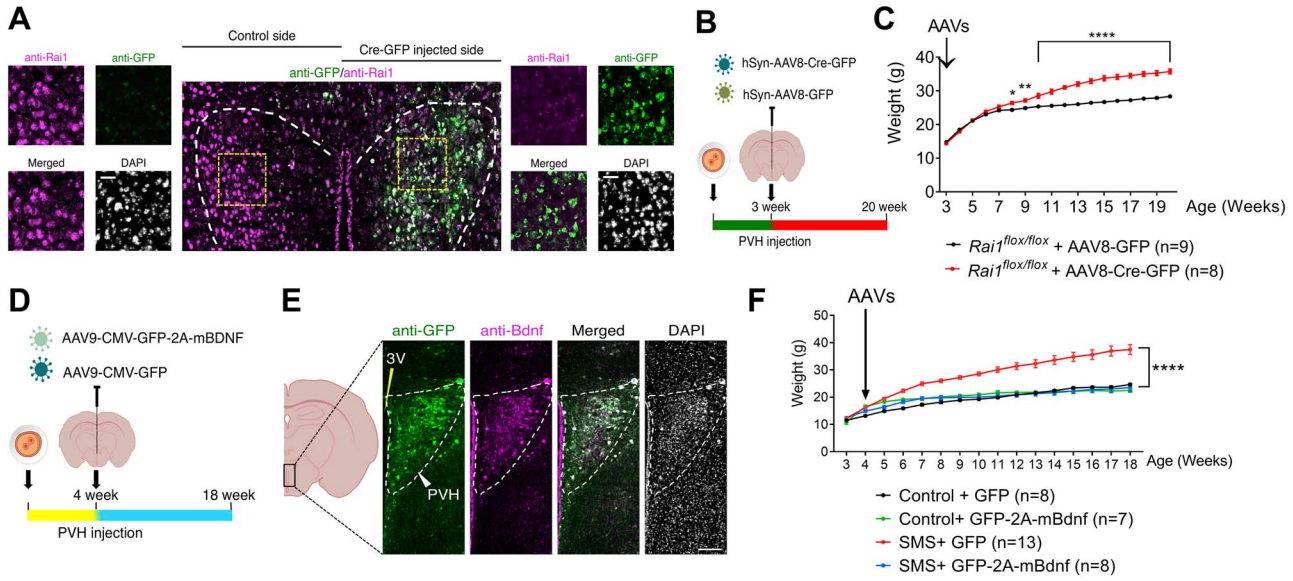

Figure 4. PVH neurons are involved in SMS-like obesity phenotype in mice. **(A)** Unilateral injection of AAV-GFP into the PVH. The GFP-Cre-injected side showed decreased Rai1 expression and ectopic GFP expression (magnified on the right). The scale bar represents 20 μm. **(B)** Schematic illustrating bilateral injections of AAVs expressing either GFP or Cre-GFP into the PVH neurons of $Rai1^{flox/flox}$ mice at 3 weeks of age. **(C)** Female $Rai1^{flox/flox}$ mice injected with AAV8-Cre-GFP showed a significant increase in body weight when compared to AAV8-GFP (Two-way analysis of variance). **(D)** Schematic depicting the injection of AAVs expressing either GFP or GFP-mBdnf into the PVH at 4 weeks of age. **(E)** Immunostaining confirming the expression of GFP and mBdnf in the PVH of a control mouse. DAPI staining indicates the nucleus. **(F)** SMS mice with AAV9-GFP-mBdnf injected in the PVH showed a significant decrease in body weight when compared to SMS mice with AAV9-GFP or AAV9-GFP-mBdnf injection. Error bars indicate SEM. $^{*}P < 0.05$, $^{**}P < 0.01$, $^{****}P < 0.0001$.

with *hBdnf* was comparable to that of their control and $hBdnf^{Tg}$ littermates (Fig. 5C). At 25 weeks of age, the mean body weight of SMS + $hBdnf^{Tg}$ mice was roughly 50% of that of their non-treated SMS littermates and was not significantly different from that of control or $hBdnf^{Tg}$ mice (Fig. 5D), demonstrating that $hBdnf^{Tg}$ reversed obesity in SMS mice. We then measured body composition using an echo magnetic resonance imaging (MRI) analyzer. The fat mass (Supplementary Material, Fig. S6A) and lean mass (Supplementary Material, Fig. S6B) weighed significantly more in SMS mice than in control, $hBdnf^{Tg}$ or SMS + $hBdnf^{Tg}$ mice. By dissecting and quantifying the levels of fat deposition in different organs, we found that SMS mice showed increased adiposity in the liver, brown adipose tissue, subcutaneous inguinal white adipose tissue, epididymal white adipose tissue and mesenteric white adipose tissue (Fig. 5E). Fat deposition levels in all organs were restored to normal levels in SMS + $hBdnf^{Tg}$ mice, as they were indistinguishable from those in control and $hBdnf^{Tg}$ mice. Finally, we measured adipocyte size using hematoxylin and eosin (H&E) staining and found that the increased adipocyte hypertrophy in SMS mice was reversed by $hBdnf^{Tg}$ expression (Fig. 5F). Together, these data indicate that hBdnf treatment reversed the obesity, abnormal fat mass, increased adiposity and adipocyte hypertrophy in SMS mice.

SMS patients show increased high-density lipoproteins (HDL), low-density lipoproteins (LDL) and triglycerides levels (33). Therefore, we analyzed the serum concentration of different types of lipids and found that SMS mice showed increased levels of HDL and LDL/very-low-density lipoprotein (VLDL) (Fig. 5G). Consistent with increased adiposity, leptin levels were significantly elevated in SMS mice (Fig. 5G). The lipid and leptin levels in SMS + $hBdnf^{Tg}$ mice were indistinguishable from control and $hBdnf^{Tg}$ mice, consistent with hBdnf treatment reversed the hypercholesterolemia and hyperleptinemia in SMS mice.

Obesity is a state of energy imbalance caused by increased food intake, reduced EE or both (19). To determine the mechanism by which $hBdnf^{Tg}$ reversed SMS-like obesity, we placed mice into the metabolic cages of a Comprehensive Lab Animal Monitoring System (CLAMS) for 24 h. Mice in different groups showed similar respiratory exchange rates (RERs), as determined by oxygen consumption and carbon dioxide production during light and dark cycles (Supplementary Material, Fig. S6C). To determine EE, we normalized oxygen consumption by lean mass because adipocytes are less metabolically active than lean tissues (34). EE levels during the light and dark phases were not significantly different among mice of different genotypes (Supplementary Material, Fig. S6D), similar to our previous findings in mice with *Rai1* deleted from Sim1 neurons (14). During the dark phase (when rodents consume more food) but not the light phase, SMS mice showed significantly greater food intake (3.47 ± 0.24 g) than control mice (2.56 ± 0.23 g, $P < 0.05$) (Supplementary Material, Fig. S6E). By contrast, SMS + $hBdnf^{Tg}$ mice showed levels of food intake similar to those of control mice (Supplementary Material, Fig. S6E). It should be noted that *post hoc* analysis did not detect significant differences in food intake between the different groups over a 24-h period (Supplementary Material, Fig. S6F), presumably because of a novelty effect in which exposure to a new environment (i.e. the CLAMS cages) overshadowed significant between-group differences. These data suggest that hBdnf reversed obesity by correcting the overfeeding behavior in SMS mice.

To explore if hBdnf treatment affects metabolic tolerance, we performed a glucose tolerance test (GTT) in fasted mice. Fasted SMS mice showed glucose levels at time 0 (before glucose injection, 8.8 ± 0.4 mM) that were significantly higher than those of the other three groups (range: 6.0–6.7 mM) (Fig. 5H). Furthermore, relative to the other three groups, SMS mice remained hyperglycemic throughout the course of the GTT (except at the

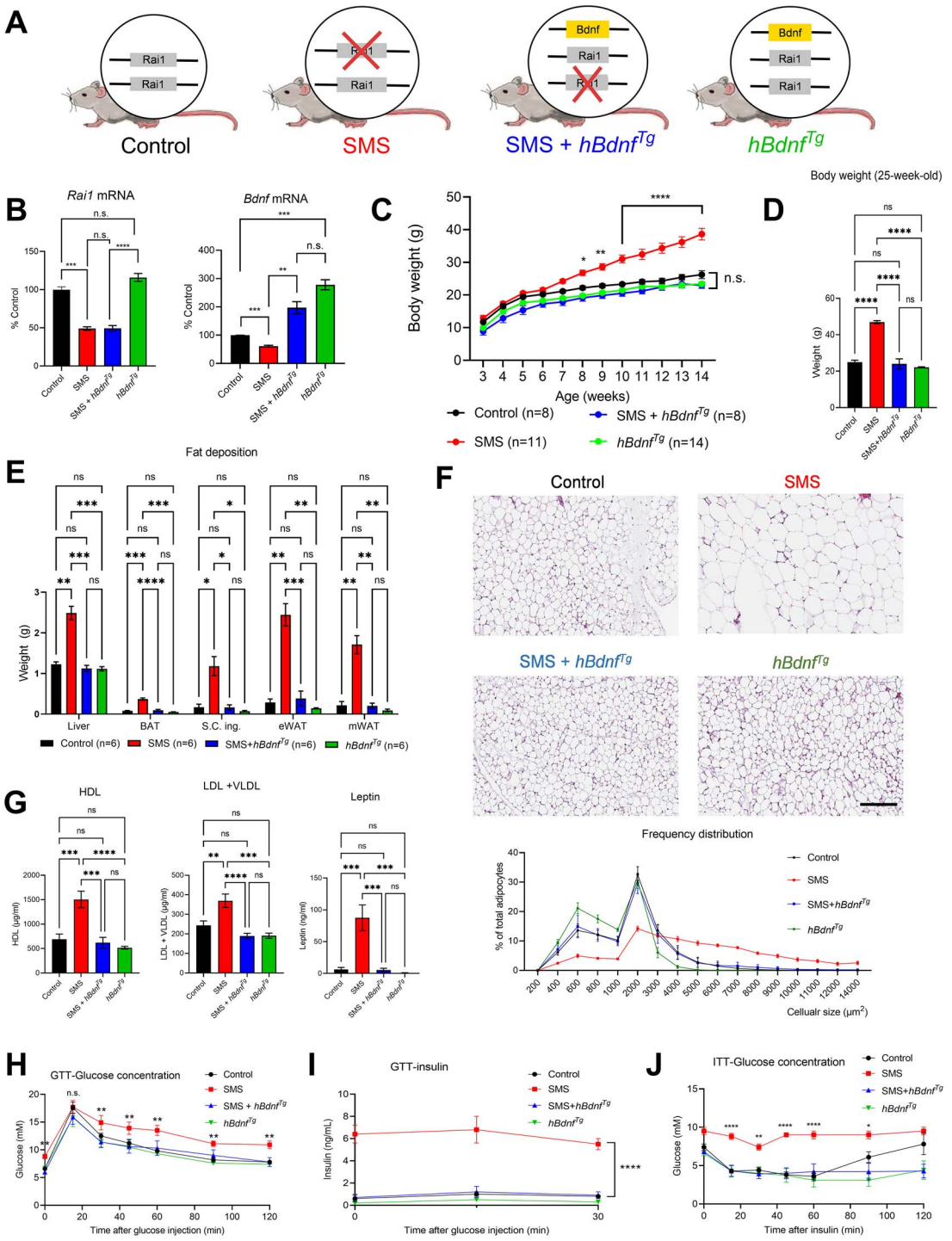

Figure 5. Ectopic expression of hBdnf reverses SMS-like obesity and metabolic features in female SMS mice. (**A**) Schematic depicting the Bdnf-STOP allele that allows Cre-dependent ectopic hBdnf expression. (**B**) Hypothalamic qRT-PCR showing that SMS mice with or without hBdnf treatment showed a 50% decrease in *Rai1* expression. The $hBdnf^{Tg}$ allele increased *Bdnf* mRNA expression by 2.7-folds (control versus $hBdnf^{Tg}$). *Bdnf* mRNA levels in SMS mice showed a 40% decrease when compared to control mice and increased by 97% after hBdnf treatment ($n = 3$ per genotype). (**C**) Body weight measurements show that hBdnf treatment reduced the body weight of SMS mice to similar levels as control and $hBdnf^{Tg}$ mice. (**D**) Body weight of four groups of mice undergoing CLAMS analysis at 25 weeks of age ($n = 6$ per genotype from **C–J**). (E) SMS mice showed increased fat deposition levels in multiple organs, which were reversed by Bdnf treatment. (F) SMS mice showed adipocyte hypertrophy, which was reversed by $hBdnf^{Tg}$. Top: Representative images of H&E staining of ependymal WAT from each group of mice. Bottom: Frequency distribution of adipocytes at each cellular size. (G) SMS showed increased HDL, LDL/VLDL and leptin levels. These parameters were restored to levels similar to those of control and $hBdnf^{Tg}$ mice by hBdnf treatment. (H) In GTT experiments, SMS mice showed higher plasma glucose levels than control mice throughout the test (except at the peak). By contrast, the glucose levels of SMS + $hBdnf^{Tg}$ mice were indistinguishable from those of control and $hBdnf^{Tg}$ mice. (I) In GTT experiments, SMS mice showed higher plasma insulin levels, which were reversed by hBdnf treatment. (J) SMS mice showed significantly higher glucose levels in ITT than in control mice. This increase was reversed by hBdnf treatment. Error bars indicate SEM. n.s. indicates not significantly different. $^{*}P < 0.05$, $^{**}P < 0.01$, $^{***}P < 0.001$, $^{****}P < 0.0001$. Scale bars: 500 μm.

peak), a difference accompanied by a higher plasma insulin concentration in SMS mice relative to the other three groups (Fig. 5I). However, for glucose levels, the area under the curve (AUC) did not significantly differ between groups (Supplementary Material, Fig. S6G), indicating normal glucose tolerance. By contrast, for insulin levels, the AUC was significantly higher in SMS mice than in the other three groups (Supplementary Material, Fig. S6H). Intriguingly, the abnormal blood glucose level and insulin secretion patterns observed in SMS mice were completely reversed by hBdnf overexpression (Fig. 5H and I). The interpretation of insulin resistance was supported by an insulin tolerance test (ITT). Specifically, fasted SMS mice showed high baseline insulin levels, which were reversed by hBdnf treatment (Supplementary Material, Fig. S6I). During the ITT, SMS mice showed blunted glucose decrement in response to insulin challenge (Supplementary Material, Fig. 5J), although the inverse AUC did not significantly differ between the groups (Supplementary Material, Fig. S6J). The insulin intolerance in SMS mice during the ITT was reversed by hBdnf treatment (Fig. 5J). Altogether, these experiments demonstrated that ectopic expression of hBdnf could reverse the obesity, adiposity, overfeeding and metabolic-like phenotypes of SMS mice.

Overexpression of *hBdnf* reverses SMS-like hyposociability in SMS mice

Prompted by the therapeutic effect of *hBdnf* in reversing SMS-like obesity and metabolic deficits, we further tested if *hBdnf* treatment could reverse hyposociability in SMS mice at 6–7 weeks of age, when they exhibit social defects (15) and have body weights comparable to those of their control littermates. We found that male SMS mice showed a robust hyposocial phenotype, withdrawing from more than 95% of face-to-face social encounters with their control littermates (Fig. 6A), consistent with previous findings (5,12,15). Remarkably, SMS + $hBdnf^{Tg}$ mice showed comparable levels of winning in the tube test against control mice (Fig. 6B) and won 70% of encounters with SMS mice (Fig. 6C). These findings indicate that SMS + $hBdnf^{Tg}$ mice show significantly better social function than SMS mice. Interestingly, $hBdnf^{Tg}$ mice showed hyposociability, losing 70% of encounters with their control littermates (Fig. 6D), suggesting that the therapeutic effect of *hBdnf* overexpression on hyposociability is specific to SMS mice.

Discussion

SMS is a neurodevelopmental disorder associated with childhood-onset obesity, maladaptive behaviors and autistic features. The goal of this study was to genetically define the temporal requirement of Rai1 and identify Rai1-dependent genes as therapeutic targets. We found that Rai1 has a continuous role in the postnatal brain to regulate energy balance by maintaining Bdnf expression and that enhancing Bdnf signaling reversed SMS-like disease features in mice. Our findings constitute the first report that normalizing the expression level of one of the many target genes of Rai1 can reverse SMS disease progression *in vivo*.

By globally deleting *Rai1* at different postnatal stages, we found that neural circuits mediating SMS-like neurobehavioral features do not require Rai1 beyond the weaning age. The lack of behavioral deficits cannot be explained by delayed symptom onset because mice with adolescent *Rai1* deletion developed SMS-like obesity without detectable neurobehavioral deficits. Remarkably, postnatal-onset Rai1 loss resulted in dose-dependent weight gain associated with overfeeding, similar to the consequences of embryonic *Rai1* deletion (5,14). At the cell-type level, we uncovered that PVH neurons depend on Rai1 expression to control food intake. Because the PVH region contains several neuronal subtypes demarcated by distinct patterns of neuropeptide expression (19), an important future direction will be to pinpoint the PVH subtype(s) responsible for mediating unbalanced energy homeostasis caused by Rai1 loss. Together, these findings suggest that SMS-like neurobehavioral features and imbalanced energy intake are temporally dissociable. The continuous requirement for Rai1 activity suggests that Rai1 reinstatement therapies should be sustained throughout life for maximal efficacy in treating SMS.

In a mouse model of PTLS, a childhood neurodevelopmental disorder associated with autism, developmental delay and neuropsychiatric problems, Rai1 overexpression during the embryonic (but not postnatal) stage is responsible for PTLS-like phenotypes (35). Normalizing Rai1 levels at conception can reverse PTLS-like disease features, but doing so at adolescence (4 weeks of age) or adulthood (12 weeks of age) cannot. Together with our study, these results suggest that *Rai1* dosage during embryonic development needs to be precisely controlled to establish proper neurobehavioral function in adulthood. Understanding the molecular function of Rai1 during embryogenesis should provide insights into the etiologies of SMS and PTLS. The importance of Rai1 during early development is further highlighted by the high lethality (>95%) of $Rai1^{-/-}$ mice *in utero* (10). A prominent challenge in the field is that while $Rai1^{+/-}$ mice genetically mimic SMS, they show limited (but highly reproducible) SMS-like disease features, such as obey and social dysfunction (13). Future exploration of other behavioral phenotypes in $Rai1^{+/-}$ mice will broaden the measurements available to assess the efficacy of therapeutic treatments.

By comparing the hypothalamic transcriptomes of mice with embryonic or postnatal *Rai1* deletions, we uncovered that Rai1 expression is required to continuously maintain *Bdnf* expression. In the hypothalamus, Bdnf is expressed by excitatory neurons located in discrete regions important for energy homeostasis, such as the PVH and VMH (24,26). Bdnf regulates feeding primarily by binding to its cognate receptor, tropomyosin receptor kinase B (TrkB), which when deleted also causes obesity (36,37). Although *Rai1* deletion affects the expression of hundreds of downstream target genes (14,38), we found that postnatal *Bdnf* gene therapy in the PVH or VMH was sufficient to reverse the obesity induced by *Rai1* haploinsufficiency. Interestingly, control and $Rai1^{+/-}$ mice with mBdnf overexpressed in the PVH showed similar body weight. By contrast, AAV delivery of mBdnf into the VMH reduced body weight independent of *Rai1* dosage. This raises the possibility that Rai1 and Bdnf signaling occur serially through a linear pathway in the PVH, while occurring in parallel in the VMH. Because Bdnf signaling can occur though retrograde, anterograde and autocrine pathways, a future challenge will be to dissect the directionality of Bdnf signaling in health and obesity. This is further complicated by the fact that many synaptically connected hypothalamic nuclei express Bdnf, TrkB or both (29). Given the pleotropic roles of Bdnf in regulating neuronal activity and structures (39), it would be important in the future to pinpoint if reduced Bdnf drives obesity by impairing the firing pattern, neuronal morphology or both in synaptically connected TrkB-expressing cells (29,40).

Patients with *BDNF* haploinsufficiency share selective phenotypic similarities with SMS patients, including obesity and impaired cognitive function (21). $Bdnf^{+/-}$ mice are obese and show hyperphagia, hyperleptinemia, hypercholesterolemia,

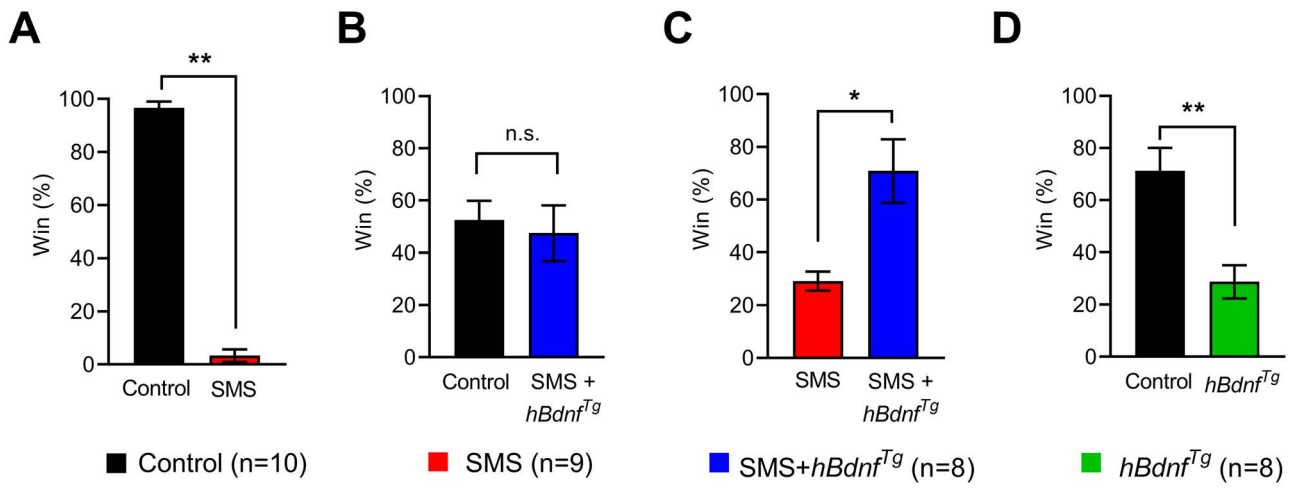

Figure 6. Global increase of human Bdnf reverses hyposociability in SMS mice. (**A**) SMS mice showed a severe social interaction deficit in the tube test, retreating from 96% of social encounters with control littermates. (**B**) SMS mice with hBdnf overexpression showed performance levels comparable to those of control littermates. (**C**) SMS mice with hBdnf overexpression behaved similar to their control littermates, winning ~50% of the social encounters against untreated SMS mice. (**D**) *hBdnf*^{Tg} mice showed impaired social interaction when encountering control mice, suggesting that hBdnf overexpression in wild-type mice has an effect distinct from that in SMS mice. Error bars indicate SEM. n.s. indicates not significantly different. $^{*}P < 0.05$, $^{**}P < 0.01$.

hyperinsulinemia and hyperglycemia (20,23). We found that SMS mice showed hyperphagia, hyperleptinemia, hypercholesterolemia, hyperinsulinemia, hyperglycemia, adipocyte hypertrophy, increased fat and lean mass, insulin resistance, all of which were reversed by globally overexpressing hBdnf. By contrast, these obesity- and metabolism-associated parameters were not significantly altered by overexpressing hBdnf in control mice. Therefore, reduced Bdnf expression is a likely key mechanism driving the weight gain induced by *Rai1* haploinsufficiency and has emerged as a promising candidate pathway to treat obesity and metabolic-like features in SMS. Future studies aimed at optimizing the therapeutic timing and duration, safety, and dosage of TrkB agonists will be important for clinical translation. Furthermore, our findings suggest that Rai1 and Bdnf expression need to be continuously maintained postnatally. If so, then Bdnf gene therapy is another potential therapeutic option because it is a one-time treatment that confers a long-term and stable effect.

The beneficial effects of hBdnf in reversing SMS-like social dysfunction are particularly exciting given the prevalent autistic features in SMS patients (4). A *de novo RAI1* point mutation (c.3440G>A) has been reported in a patient associated with autism and some SMS-like features (41). Interestingly, the RAI1 protein carrying this mutation showed decreased transcriptional activity to promote Bdnf expression *in vitro* (41). Our findings also suggest that similar to Rai1, balanced Bdnf levels are important for social function because increasing hBdnf expression reversed social dysfunction in SMS mice, but induced a hyposocial behavior in control mice.

Several important questions need to be answered to determine whether Bdnf is a potential candidate for treating SMS. For example, the neuronal subtype(s) and brain region(s) responsible for the therapeutic effect of Bdnf remain to be defined. Our previous work showed that deleting one copy of *Rai1* in either glutamatergic or GABAergic neurons was sufficient to induce hyposociability (15), suggesting that Bdnf could reverse social interaction through multiple cell types. Bdnf is also a key regulator of axonal/dendritic development as well as synaptic function and plasticity (42,43). Therefore, we also need to carefully evaluate how Bdnf therapy reverses SMS-like disease features at the cellular and synaptic levels. Collectively, our work provides genetic evidence for a postnatal function of Rai1 and suggests a functional interaction between Rai1 and Bdnf in SMS pathogenesis that could potentially be leveraged for therapeutic interventions.

Materials and Methods

Mouse breeding and husbandry

All procedures were performed in accordance with the guidelines of the Canadian Council on Animal Care and the Montreal General Hospital Facility Animal Care Committee, with the appropriate approved protocols for animal use. Mice were housed in groups on a 12-h light/12-h dark cycle with *ad libitum* access to food and water. *Rai1*$^{flox/flox}$ mice were maintained in the CD1 and C57BL/6J background by backcrossing for more than 10 generations. *Ubc*^{CreERT2} (16), *Nestin*^{Cre} (18), *Bdnf*^{STOP} (32) and *ActB*^{Cre} (31) mice were maintained in the C57BL/6J background. *Rai1*$^{+/-}$ mice were generated by crossing *Rai1*$^{flox/flox}$ mice with the germline *ActB*^{Cre} line to delete *Rai1*. For consistency, all experiments were conducted using F1 hybrids of CD1 and C57BL/6J parents. To measure food intake over a 1-week period, food was weighed daily prior to placement in the cage. The next day, food remaining in the hopper and any significant spillage inside the cage were combined and weighed. The amount of food consumed was averaged over 7 days.

TAM treatment

To delete *Rai1* at 3 and 8 weeks of age, control (*Ubc*^{CreERT2} and *Rai1*$^{flox/+}$), *Ubc*^{CreERT2};*Rai1*$^{flox/+}$ and *Ubc*^{CreERT2};*Rai1*^{CKO} mice received five intraperitoneal (IP) injections of TAM (100 mg/kg, Sigma-Aldrich, United States) over 10 days (i.e. injections occurred every other day). TAM was dissolved in corn oil at a concentration of 20 mg/ml, protected from light by aluminum foil, aliquoted and stored at −20°C for no more than 2 weeks.

Immunostaining and immunoblotting

Mouse brains were rapidly dissected, immersed in Optimal Cutting Temperature compound (Thermo-Fisher, United States) and frozen by immersion in a dry ice/ethanol bath. Sections were

washed in a phosphate-buffered saline (PBS) solution and incubated for 10 min at −20°C in pre-cooled acetone, washed again in PBS and then blocked for 2 h at room temperature in 10% normal donkey serum (NDS) in PBS. Samples were further incubated overnight at 4°C with anti-Rai1 antibody (prepared in-house, 1:500) in 10% NDS/PBS. The next day, the slides were incubated for 2–3 h at room temperature with secondary antibodies in 10% NDS in PBS and coverslipped in DAPI-containing Fluoromount-G (SouthernBiotech, United States). For immunostaining experiments using anti-Bdnf (Abcam, United Kingdom, ab108319) and anti-GFP (Abcam, United Kingdom, ab13970) antibodies, mice were perfused with 4% paraformaldehyde and then processed similarly.

An immunoblotting assay (western blot analysis) was used to quantify Rai1 protein levels. Protein was extracted and separated by SDS-PAGE gel and then transferred onto nitrocellulose membranes. Membranes were cut into two portions, blocked in 5% milk in Tris-buffered saline (TBS) for 1 h and incubated at 4°C with anti-Rai1 antibody (1:500) or anti-Gapdh antibody (ab9485, Abcam, United Kingdom; 1:10 000) in TBS containing 0.1% Tween 20 (TBS-T) with 2% milk overnight. The next day, membranes were washed with TBS-T and incubated with secondary antibodies conjugated with horseradish peroxidase (Thermo-Fisher, United States). Finally, membranes were incubated with ECL substrates and then imaged using a Bio-Rad ChemiDoc imager.

RNA-seq and qRT-PCR

RNA-seq and qRT-PCR were used to measure gene expression changes caused by Rai1 loss. Hypothalamic tissues of 30-week-old female $Ubc^{CreERT2}$;$Rai1^{CKO}$ mice and their $Ubc^{CreERT2}$ control littermates (injected with TAM at 3 weeks of age) were used for RNA-seq experiments. Total RNA was extracted by TRIzol reagent and phenol-chloroformisoamyl alcohol (Thermo-Fisher, United States). The residual DNA was removed with on-column DNase digestion (Qiagen, Germany) and RNA was further purified using an RNeasy Kit (Qiagen, Germany). Ribosomal RNA was depleted with Ribo-Zero rRNA removal kits (Illumina, United States). The RNA-seq libraries were sequenced by a HiSeq 2500 sequencing system (Illumina, United States). The raw sequences were processed as previously described (14). Briefly, the adaptor sequences were removed by cutadapt and then aligned to mouse reference genome (mm9) using Tophat2 (44). The gene expression level was quantified using the R package DEGseq (v0.50.1) according to the RefGene annotation from the UCSC genome browser database (the longest isoforms were selected when there were multiple transcripts) (45). Differentially expressed genes were identified by the R package DESeq2 (46) and those with a false discovery rate (FDR) of less than 0.1 were selected for downstream comparison and gene ontology annotation. Differentially expressed genes with an FDR of less than 0.1 in either group were selected and changes were compared to the results from our previous study (14). qRT-PCR was performed with independently isolated samples. After isolation of total RNA, mRNA was reverse-transcribed with the SuperScript III First-Strand Synthesis System (Thermo-Fisher, United States). Quantitative PCR reactions were conducted using SsoFast EvaGreen Supermix on a Bio-Rad qPCR system. The RNA-seq data are available at GEO (GSE149952).

Stereotaxic injection

Mice were anesthetized with isoflurane and ear-barred in a stereotaxic instrument (David Kopf, United States). AAVs (0.5 µl) were administered bilaterally into the PVH using the following coordinates relative to bregma: −0.6 mm anteroposterior (AP); ±0.35 mm mediolateral (ML) and −5.52 mm dorsoventral (DV). VMH injections were done using the following coordinates relative to the bregma: −1.58 mm AP; ±0.4 mm ML and −5.7 mm DV. The following AAVs were used: AAV8-hSyn-Cre-GFP (UNC, United States), AAV8-hSyn-GFP (UNC, United States), AAV9-CMV-GFP-2A-mBDNF (AAV-253926, Vector Biosystems Inc, United States) and AAV9-CMV-GFP (Vector Biosystems Inc, United States).

Metabolic profiling

Chow-fed female control mice, $Rai1^{+/-}$ mice with or without hBdnf overexpression and control mice with hBdnf overexpression ($n = 6$ per genotype) were used for metabolic profiling at 23–25 weeks of age. The respiratory exchange rate (RER) and EE were measured using indirect calorimetry in the metabolic cages of a CLAMS (Columbus Instruments, United States). Animals were singly housed in the CLAMS apparatus at 21°C (70°F) in a light–dark cycle matching their housing conditions for 24 h (acclimation), followed by 48 h of measurement. EE was normalized by lean mass.

Serum lipid panel determination. A fluorimetric assay kit (cat# ab65390, Abcam, United Kingdom) was used for the measurement of serum HDL and LDL/VLDL levels. The kit was used according to the manufacturer's instructions except that half-area black 96-well microplates were used. Fluorescence at 535/587 nm (Ex/Em) was recorded using the Ensight instrument (PerkinElmer, United States). A fresh standard curve (0 and 10 µg/ml) was made for each microplate to be able to precisely quantify HDL and LDL/VLDL cholesterol levels of serum samples. Standards and samples were loaded and analyzed in duplicate.

Adipose tissue histology and analysis. Ependymal WAT was excised immediately after euthanasia and fixed (10% formalin in PBS), dehydrated, embedded in paraffin and sectioned. For each animal, two 5-µm thick sections were stained with hematoxylin and eosin and captured at 20× optical magnification with an Aperio ScanScope CS slide scanner (Leica Biosystems, Germany). Images were recorded in jpeg at 4× magnification using ImageScope software version 12.3.2.5030 (Leica Biosystems, Germany) and were manually clean to remove non-adipose tissues (e.g. lymph nodes). Adipocyte size and number were determined utilizing an automated method using the jpeg images and Fiji (ImageJ) version 2.1.0/1.53c (National Institutes of Health, United States) with the Adiposoft plugin version 1.16 (47). The following Adiposoft settings were used: cells on edges were excluded, and minimum and maximum cell diameters were 20 and 300 µm, respectively. A 2.49-µm per pixel value was determined experimentally using the Aperio scale bar and used for Adiposoft. To ensure accuracy of measurement, two images of each animal were analyzed blindly representing >1600 cells per mouse and >9100 cells per condition. Adipocyte size frequencies were computed using the frequency function in Excel.

Body composition. Total fat and lean mass were assessed using a nuclear echo MRI whole-body composition analyzer. Liver, brown adipose, visceral (mesenteric) and subcutaneous (inguinal) tissues, as well as ependymal fat pads, were collected and weighed using an analytical scale (Sartorius, Germany).

Glucose tolerance. Experimental mice were food-deprived for 5 h with *ad libitum* access to water. A bolus of glucose (1.5 g/kg of lean body weight) was administered via an IP injection and glycemia

was measured from blood sampled at the tail vein using an Accuchek Performa glucometer at T0 (before the injection) as well as at 15, 30, 45, 60, 90 and 120 min (after the injection). Tail vein blood samples were collected via a capillary for insulin assays at T0, 15 and 30 min.

Insulin tolerance. Experimental mice were food-deprived for 5 h with *ad libitum* access to water. A bolus of insulin (1 U/kg of lean body weight) was administered via an IP injection and glycemia was measured from blood sampled at the tail vein using a Accuchek Performa glucometer at T0 (before the injection), as well as at 15, 30, 45, 60, 90 and 120 min (after the injection). Tail vein blood samples were collected via a capillary for insulin assays at T0.

Behavioral tests

All behavioral experiments were performed during the light period of the light/dark cycle. Mice were habituated to handling for 3 days prior to the first behavioral tests. At least 1 day was given between assays for the mice to recover. Randomization of mice was performed, and experimenters were blind to the mouse genotype during behavioral testing and data analysis. We chose the following behavioral tests for *Rai1* heterozygous and homozygous knockout mice because the results have been reproduced by different research groups, including ours (12–15).

Tube test. We used a tube test to measure social interaction. Mice were housed in cages in the testing environment for 1 day before training. On each of two training days, each mouse passed through the tube for 10 trials (five times from each side, without opponents), which helped familiarize the mice with walking through the tube and knowing that the tube was safe. On the test days, two mice of different genotypes were placed at the two ends of the tube and released simultaneously to meet in the middle of the tube. The mouse that retreated first from the tube was designated as the loser. To avoid measuring social hierarchy established between cage mates, the animals used for the tube test were housed with littermates of the same genotype and encountered unfamiliar mice of differing genotype in the tube test.

Pole test. We used a vertical pole descent test to measure motor function. Mice were placed at the top of a coarse, vertical wooden pole (1 cm in diameter, 55 cm in height), and the time required to descend was recorded. After a practice trial, four test trials were conducted at an inter-trial interval of ∼2 min. If the mouse did not descend, or either dropped or slipped down the pole without climbing down, a descent time of 60 s was recorded.

Fear conditioning test. On day 1 (training), a mouse was placed in Context A and after 3 min, presented with a tone (75 dB, 2 kHz, 20 s) followed by a foot-shock (0.5 mA, 2 s) 18 s later. The mouse received a total of five tone-shock pairings at an inter-tone interval (from the end of one tone to the start of the next tone) of 80 s. On day 2 (contextual recall), the mouse was placed in Context A for 5 min without any tone presentation. On day 3 (cued recall), the mouse was placed for 3 min in Context B, which had cues different from those in Context A. The mouse was subsequently presented with the same tones (at an 80-s inter-tone interval) without any shocks. Freezing, defined as the complete lack of motion for at least 0.75 s, was quantified for all 3 days using an automated video scoring system (FreezeFrame, Actimetrics, United States).

Statistical tests

All data were statistically analyzed using GraphPad Prism 9 software, and *P*-values less than 0.05 were considered significant. The levels of significance are indicated as follows: $^{*}<0.05$, $^{**}<0.01$, $^{***}<0.001$ and $^{****}<0.0001$. Statistical analysis was performed using Student's *t*-test or One- or Two-way analysis of variance with Bonferroni's *post hoc* correction for multiple comparisons.

Supplementary Material

Supplementary Material is available at *HMG* online.

Acknowledgements

We acknowledge the support from the Jerome LeJeune Foundation and SMS Research Foundation. We thank Dr Qiang Chang at the University of Wisconsin-Madison and Dr Rudolf Jaenisch at the Whitehead Institute, Massachusetts Institute of Technology, for providing the $Bdnf^{STOP/+}$ mice. We thank the Centre de recherche du CHUM (CRCHUM) rodent metabolic phenotyping core facility for metabolic studies. Wei-Hsiang Huang is an Azrieli Centre for Autism Research (ACAR) Researcher and supported by the Fonds de recherche du Québec – Santé.

Conflict of Interest statement. All authors declare that they have no competing interests.

Funding

We acknowledge the support from the Jerome LeJeune Foundation and Smith-Magenis syndrome Research Foundation.

References

1. Slager, R.E., Newton, T.L., Vlangos, C.N., Finucane, B. and Elsea, S.H. (2003) Mutations in RAI1 associated with Smith-Magenis syndrome. *Nat. Genet.*, **33**, 466–468.
2. Boot, E., Linders, C.C., Tromp, S.H., van den Boogaard, M.J. and van Eeghen, A.M. (2021) Possible underreporting of pathogenic variants in RAI1 causing Smith-Magenis syndrome. *Am. J. Med. Genet. A*, 1–3. PMID: 34089220.
3. Smith, A.C., McGavran, L., Robinson, J., Waldstein, G., Macfarlane, J., Zonona, J., Reiss, J., Lahr, M., Allen, L. and Magenis, E. (1986) Interstitial deletion of (17) (p11.2p11.2) in nine patients. *Am. J. Med. Genet.*, **24**, 393–414.
4. Laje, G., Morse, R., Richter, W., Ball, J., Pao, M. and Smith, A.C. (2010) Autism spectrum features in Smith-Magenis syndrome. *Am. J. Med. Genet. C: Semin. Med. Genet.*, **154C**, 456–462.
5. Burns, B., Schmidt, K., Williams, S.R., Kim, S., Girirajan, S. and Elsea, S.H. (2010) Rai1 haploinsufficiency causes reduced Bdnf expression resulting in hyperphagia, obesity and altered fat distribution in mice and humans with no evidence of metabolic syndrome. *Hum. Mol. Genet.*, **19**, 4026–4042.
6. Edelman, E.A., Girirajan, S., Finucane, B., Patel, P.I., Lupski, J.R., Smith, A.C. and Elsea, S.H. (2007) Gender, genotype, and phenotype differences in Smith-Magenis syndrome: a meta-analysis of 105 cases. *Clin. Genet.*, **71**, 540–550.

7. Potocki, L., Chen, K.S., Park, S.S., Osterholm, D.E., Withers, M.A., Kimonis, V., Summers, A.M., Meschino, W.S., Anyane-Yeboa, K., Kashork, C.D. *et al.* (2000) Molecular mechanism for duplication 17p11.2- the homologous recombination reciprocal of the Smith-Magenis microdeletion. *Nat. Genet.*, **24**, 84–87.
8. Zhang, F., Potocki, L., Sampson, J.B., Liu, P., Sanchez-Valle, A., Robbins-Furman, P., Navarro, A.D., Wheeler, P.G., Spence, J.E., Brasington, C.K. *et al.* (2010) Identification of uncommon recurrent Potocki-Lupski syndrome-associated duplications and the distribution of rearrangement types and mechanisms in PTLS. *Am. J. Hum. Genet.*, **86**, 462–470.
9. Javed, S., Selliah, T., Lee, Y.J. and Huang, W.H. (2020) Dosage-sensitive genes in autism spectrum disorders: from neurobiology to therapy. *Neurosci. Biobehav. Rev.*, **118**, 538–567.
10. Bi, W., Ohyama, T., Nakamura, H., Yan, J., Visvanathan, J., Justice, M.J. and Lupski, J.R. (2005) Inactivation of Rai1 in mice recapitulates phenotypes observed in chromosome engineered mouse models for Smith-Magenis syndrome. *Hum. Mol. Genet.*, **14**, 983–995.
11. Fragoso, Y.D., Stoney, P.N., Shearer, K.D., Sementilli, A., Nanescu, S.E., Sementilli, P. and McCaffery, P. (2015) Expression in the human brain of retinoic acid induced 1, a protein associated with neurobehavioural disorders. *Brain Struct. Funct.*, **220**, 1195–1203.
12. Rao, N.R., Abad, C., Perez, I.C., Srivastava, A.K., Young, J.I. and Walz, K. (2017) Rai1 haploinsufficiency is associated with social abnormalities in mice. *Biology (Basel)*, **6**, 1–13.
13. Bi, W., Yan, J., Shi, X., Yuva-Paylor, L.A., Antalffy, B.A., Goldman, A., Yoo, J.W., Noebels, J.L., Armstrong, D.L., Paylor, R. *et al.* (2007) Rai1 deficiency in mice causes learning impairment and motor dysfunction, whereas Rai1 heterozygous mice display minimal behavioral phenotypes. *Hum. Mol. Genet.*, **16**, 1802–1813.
14. Huang, W.H., Guenthner, C.J., Xu, J., Nguyen, T., Schwarz, L.A., Wilkinson, A.W., Gozani, O., Chang, H.Y., Shamloo, M. and Luo, L. (2016) Molecular and neural functions of Rai1, the causal gene for Smith-Magenis syndrome. *Neuron*, **92**, 392–406.
15. Huang, W.H., Wang, D.C., Allen, W.E., Klope, M., Hu, H., Shamloo, M. and Luo, L. (2018) Early adolescent Rai1 reactivation reverses transcriptional and social interaction deficits in a mouse model of Smith-Magenis syndrome. *Proc. Natl. Acad. Sci. U. S. A.*, **115**, 10744–10749. PMID: 30275311.
16. Ruzankina, Y., Pinzon-Guzman, C., Asare, A., Ong, T., Pontano, L., Cotsarelis, G., Zediak, V.P., Velez, M., Bhandoola, A. and Brown, E.J. (2007) Deletion of the developmentally essential gene ATR in adult mice leads to age-related phenotypes and stem cell loss. *Cell Stem Cell*, **1**, 113–126.
17. Mei, Y., Monteiro, P., Zhou, Y., Kim, J.A., Gao, X., Fu, Z. and Feng, G. (2016) Adult restoration of Shank3 expression rescues selective autistic-like phenotypes. *Nature*, **530**, 481–484.
18. Tronche, F., Kellendonk, C., Kretz, O., Gass, P., Anlag, K., Orban, P.C., Bock, R., Klein, R. and Schutz, G. (1999) Disruption of the glucocorticoid receptor gene in the nervous system results in reduced anxiety. *Nat. Genet.*, **23**, 99–103.
19. Andermann, M.L. and Lowell, B.B. (2017) Toward a wiring diagram understanding of appetite control. *Neuron*, **95**, 757–778.
20. Kernie, S.G., Liebl, D.J. and Parada, L.F. (2000) BDNF regulates eating behavior and locomotor activity in mice. *EMBO J.*, **19**, 1290–1300.
21. Gray, J., Yeo, G.S., Cox, J.J., Morton, J., Adlam, A.L., Keogh, J.M., Yanovski, J.A., El Gharbawy, A., Han, J.C., Tung, Y.C. *et al.* (2006) Hyperphagia, severe obesity, impaired cognitive function, and hyperactivity associated with functional loss of one copy of the brain-derived neurotrophic factor (BDNF) gene. *Diabetes*, **55**, 3366–3371.
22. Han, J.C., Liu, Q.R., Jones, M., Levinn, R.L., Menzie, C.M., Jefferson-George, K.S., Adler-Wailes, D.C., Sanford, E.L., Lacbawan, F.L., Uhl, G.R. *et al.* (2008) Brain-derived neurotrophic factor and obesity in the WAGR syndrome. *N. Engl. J. Med.*, **359**, 918–927.
23. Lyons, W.E., Mamounas, L.A., Ricaurte, G.A., Coppola, V., Reid, S.W., Bora, S.H., Wihler, C., Koliatsos, V.E. and Tessarollo, L. (1999) Brain-derived neurotrophic factor-deficient mice develop aggressiveness and hyperphagia in conjunction with brain serotonergic abnormalities. *Proc. Natl. Acad. Sci. U. S. A.*, **96**, 15239–15244.
24. An, J.J., Liao, G.Y., Kinney, C.E., Sahibzada, N. and Xu, B. (2015) Discrete BDNF neurons in the paraventricular hypothalamus control feeding and energy expenditure. *Cell Metab.*, **22**, 175–188.
25. Balthasar, N., Dalgaard, L.T., Lee, C.E., Yu, J., Funahashi, H., Williams, T., Ferreira, M., Tang, V., McGovern, R.A., Kenny, C.D. *et al.* (2005) Divergence of melanocortin pathways in the control of food intake and energy expenditure. *Cell*, **123**, 493–505.
26. Unger, T.J., Calderon, G.A., Bradley, L.C., Sena-Esteves, M. and Rios, M. (2007) Selective deletion of Bdnf in the ventromedial and dorsomedial hypothalamus of adult mice results in hyperphagic behavior and obesity. *J. Neurosci.*, **27**, 14265–14274.
27. Liao, G.Y., An, J.J., Gharami, K., Waterhouse, E.G., Vanevski, F., Jones, K.R. and Xu, B. (2012) Dendritically targeted Bdnf mRNA is essential for energy balance and response to leptin. *Nat. Med.*, **18**, 564–571.
28. Dhillon, H., Zigman, J.M., Ye, C., Lee, C.E., McGovern, R.A., Tang, V., Kenny, C.D., Christiansen, L.M., White, R.D., Edelstein, E.A. *et al.* (2006) Leptin directly activates SF1 neurons in the VMH, and this action by leptin is required for normal body-weight homeostasis. *Neuron*, **49**, 191–203.
29. Xu, B. and Xie, X. (2016) Neurotrophic factor control of satiety and body weight. *Nat. Rev. Neurosci.*, **17**, 282–292.
30. Cao, L., Lin, E.J., Cahill, M.C., Wang, C., Liu, X. and During, M.J. (2009) Molecular therapy of obesity and diabetes by a physiological autoregulatory approach. *Nat. Med.*, **15**, 447–454.
31. Lewandoski, M., Meyers, E.N. and Martin, G.R. (1997) Analysis of Fgf8 gene function in vertebrate development. *Cold Spring Harb. Symp. Quant. Biol.*, **62**, 159–168.
32. Chang, Q., Khare, G., Dani, V., Nelson, S. and Jaenisch, R. (2006) The disease progression of Mecp2 mutant mice is affected by the level of BDNF expression. *Neuron*, **49**, 341–348.
33. Smith, A.C., Gropman, A.L., Bailey-Wilson, J.E., Goker-Alpan, O., Elsea, S.H., Blancato, J., Lupski, J.R. and Potocki, L. (2002) Hypercholesterolemia in children with Smith-Magenis syndrome: del (17) (p11.2p11.2). *Genet. Med.*, **4**, 118–125.
34. Himms-Hagen, J. (1997) On raising energy expenditure in ob/ob mice. *Science*, **276**, 1132–1133.
35. Cao, L., Molina, J., Abad, C., Carmona-Mora, P., Cárdenas Oyarzo, A., Young, J.I. and Walz, K. (2014) Correct developmental expression level of Rai1 in forebrain neurons is required for control of body weight, activity levels and learning and memory. *Hum. Mol. Genet.*, **23**, 1771–1782.
36. Liao, G.Y., Kinney, C.E., An, J.J. and Xu, B. (2019) TrkB-expressing neurons in the dorsomedial hypothalamus are

necessary and sufficient to suppress homeostatic feeding. *Proc. Natl. Acad. Sci. U. S. A.*, **116**, 3256–3261.
37. An, J.J., Kinney, C.E., Tan, J.W., Liao, G.Y., Kremer, E.J. and Xu, B. (2020) TrkB-expressing paraventricular hypothalamic neurons suppress appetite through multiple neurocircuits. *Nat. Commun.*, **11**, 1729.
38. Garay, P.M., Chen, A., Tsukahara, T., Rodriguez Diaz, J.C., Kohen, R., Althaus, J.C., Wallner, M.A., Giger, R.J., Jones, K.S., Sutton, M.A. *et al.* (2020) RAI1 regulates activity-dependent nascent transcription and synaptic scaling. *Cell Rep.*, **32**, 108002.
39. Park, H. and Poo, M.M. (2013) Neurotrophin regulation of neural circuit development and function. *Nat. Rev. Neurosci.*, **14**, 7–23.
40. Podyma, B., Parekh, K., Guler, A.D. and Deppmann, C.D. (2021) Metabolic homeostasis via BDNF and its receptors. *Trends Endocrinol. Metab.*, **14**, 488–499.
41. Abad, C., Cook, M.M., Cao, L., Jones, J.R., Rao, N.R., Dukes-Rimsky, L., Pauly, R., Skinner, C., Wang, Y., Luo, F. *et al.* (2018) A rare de novo RAI1 gene mutation affecting BDNF-enhancer-driven transcription activity associated with autism and atypical Smith-Magenis syndrome presentation. *Biology (Basel)*, **7**, 1–11.
42. Chao, M.V. (2003) Neurotrophins and their receptors: a convergence point for many signalling pathways. *Nat. Rev. Neurosci.*, **4**, 299–309.
43. Huang, E.J. and Reichardt, L.F. (2001) Neurotrophins: roles in neuronal development and function. *Annu. Rev. Neurosci.*, **24**, 677–736.
44. Kim, D., Pertea, G., Trapnell, C., Pimentel, H., Kelley, R. and Salzberg, S.L. (2013) TopHat2: accurate alignment of transcriptomes in the presence of insertions, deletions and gene fusions. *Genome Biol.*, **14**, R36.
45. Wang, L., Feng, Z., Wang, X., Wang, X. and Zhang, X. (2010) DEGseq: an R package for identifying differentially expressed genes from RNA-seq data. *Bioinformatics*, **26**, 136–138.
46. Love, M.I., Huber, W. and Anders, S. (2014) Moderated estimation of fold change and dispersion for RNA-seq data with DESeq2. *Genome Biol.*, **15**, 550.
47. Miguel Galarraga, Javier Campión, Arrate Muñoz-Barrutia, Noemí Boqué, Haritz Moreno, José Alfredo Martínez, Fermín Milagro, Carlos Ortiz-de-Solórzano (2012) Adiposoft: automated software for the analysis of white adipose tissue cellularity in histological sections. *J. Lipid Res.*, **53**(12), 2791–2796. PMID: 22993232.